CHEMICAL ENGINEERING TRANSACTIONS
VOL. 71, 2018
A publication of AIDIC
The Italian Association of Chemical Engineering
Online at www.aidic.it/cet
Guest Editors: Xiantang Zhang, Songrong Qian, Jianmin Xu

ISBN 978-88-95608-68-6; **ISSN** 2283-9216
DOI: 10.3303/CET1871037

Characterization of N-doped TiO2 Pillared Clay and Its Photocatalytic Performance under Visible Light

Jinghong Zhang, Shuqin Wang*, Yixiao Xie and Jian Gao

School of Environmental Science and Engineering, North China Electric Power University, Baoding 071003, China
wsqhg@163.com

To measure the photocatalytic performance of N-doped TiO2-pillared clay nanocomposites (N-TiO2-PILC) for Cr(VI) removal under visible light, this paper prepares N-TiO2-PILC samples by sol-gel method and characterized them by scanning electron microscopy (SEM), X-ray diffraction (XRD), Brunauer–Emmett–Teller (BET) analysis and energy-dispersive X-ray spectroscopy (EDS). The author also explored the preparation conditions, settleability and reusability of the samples. The results show that N-TiO2-PILC had uniform pore size distribution, a large specific surface area (SSA) and an anatase crystal structure. The pillaring successfully introduces TiO2 particles into the clay, giving the composites a uniform interlayer structure. In addition, the optimal acid-base ratio and Ti/ clay ratio were determined as 3:1mL/mL and 15:1mmol/g, respectively; the optimal calcination temperature was proved to be 500 ºC. The research findings shed new light on the removal of Cr(VI) in water under visible light.

1. Introduction

Recent years has seen environmental pollution growing into a global problem, which attracts much attention from the academic field. Among the various pollution control techniques, photocatalysis stands out with its high efficiency and low energy consumption (Wang et al., 2018). As a typical photocatalyst, TiO2 is often doped with other elements to improve visible light absorption and photocatalytic activity. However, the application of TiO2 is severely limited by the small specific surface area (SSA) and high electron-hole recombination rate.

Many scholars have attempted to solve the problem through compound modification. For example, Zhou et al. (2017) successfully synthesized TiO2/Co-g-C3N4 composites by in-situ solvothermal generation, which improved the photocatalytic activity for phenol degradation. Hu et al. (2017) prepared TiO2/reduced graphene oxide nanocomposites, aiming to offset the limited SSA of TiO2 with the super large SSA of graphene. However, there is little report on the effect of nature clay on TiO2 modification. Nature clay has a layered structure. The interlayer cation ions can be replaced by TiO2 particles (Xu and Zhang, 2017; Han et al., 2018). After pillaring, the TiO2/clay composites enjoy a large SSA, and the electron transfer between the two materials can inhibit the electron-hole recombination.

In light of the above, this paper prepares N-doped TiO2-pillared clay nanocomposites (hereinafter referred to as the N-TiO2-PILC) by sol-gel method; then, the samples were characterized by scanning electron microscopy (SEM), X-ray diffraction (XRD), Brunauer–Emmett–Teller (BET) analysis and energy-dispersive X-ray spectroscopy (EDS), with the aim to measure its photocatalytic performance for Cr(VI) removal under visible light. The author also explored the preparation conditions, settleability and reusability of the sample.

2. Methodology

2.1 Materials

The nature clay was collected from China's south-eastern Fujian Province. The cation exchange capacity of the nature clay was determined as 71.26 mequiv/100g by X-ray fluorescence spectroscopy, suggesting a potential to accept Ti ions into the interlayers. The following reagents were purchased from Tianjin Kemiou Chemical Reagent Co., Ltd.: butyl titanate (C16H36O4Ti), hexamethylenetetramine (C6H12N4), sodium

Please cite this article as: Zhang J., Wang S., Xie Y., Gao J., 2018, Characterization of n-doped tio2 pillared clay and its photocatalytic performance under visible light, Chemical Engineering Transactions, 71, 217-222 DOI:10.3303/CET1871037

hexametaphosphate ((NaPO3)6), sodium hydroxide (NaOH), glacial acetic acid (CH3COOH), absolute ethanol (C2H5OH), nitric acid (HNO3), sulfuric acid (H2SO4), phosphoric acid (H3PO4) and solid potassium dichromate (K2Cr2O7). The above chemicals were of analytical grade and used without further purification.

2.2 Catalysts preparation

Pillaring agent: 8.5mL C16H36O4Ti and 0.98g C6H12N4 (as N source) were added to 10mL C2H5OH. The mixture was stirred for 20min to form solution A. Then, 20mL HNO3 (1M) was mixed with 5mL C2H5OH to form solution B. Next, solution A was slowly dripped into solution B and stirred for 90min, forming the pillaring agent.
Clay suspension: To begin with, 50g clay (size: 200mesh) was added into 150mL (NaPO3)6 solution (0.2%) and the mixture was strongly stirred for 1h. After standing for another hour, the mixture was centrifuged for 10min. The precipitate was then dried and ground into powder. Next, a certain amount of the powder and the NaOH solution (1mol/L) were added into 170mL deionized water. The mixture was stirred quickly for 30min and vibrated using ultrasound for 5min to form the clay suspension.
Sample preparation: The pillaring agent was dripped into the clay suspension and stirred strongly for 3h. The mixture was aged for 1d and then centrifuged for 10min. The resulting precipitate was then calcined in a muffle furnace to product the finial sample, denoted as N-TiO2-PILC.

2.3 Instruments

The microstructure of the sample was observed by a KYKY-2800B scanning electron microscope (Madell Tech, China) with a speed voltage of 5kV. The crystal structure was examined by a Y2000 X-ray diffractometer (Dandong, China) with Cu Kα radiation. The SSA and porosity were measured by a TriStarII 3020 BET analyser (Mike, US). The elements and chemical composition of the catalyst was determined using an energy dispersive spectroscope (NORAN Instruments, US).

2.4 Photocatalytic experiments

The photocatalytic experiments were carried out in a self-made reactor equipped with a 65W fluorescent at room temperature. 1g catalyst was added into 200mL Cr(VI) solution (3mg/L) under magnetic stirring to investigate the photocatalytic performance. The pH of the solution was adjusted to 3 before reaction. To ensure the adsorption equilibrium on catalyst surface, the suspensions were kept in darkness for 30min before a 90min-long illumination. At 30min intervals, 10mL aliquot of the suspensions was withdrawn to measure the instant Cr(VI) concentration via the diphenylcarbazide spectrophotometric method (GB 7467-87). The removal efficiency was determined by the difference between the initial and instant Cr(VI) concentrations. The total chromium was also measured by the said method (GB 7466-87) to determine the amount of Cr(III) in water. Batch experiments were conducted to explore the optimal preparation conditions, settleability and reusability of N-TiO2-PILC.

3. Sample Characterization

3.1 SEM analysis

Figure 1 shows the morphology of nature clay (left) and N-TiO2-PILC (right). After pillaring, the TiO2 nanoparticles were evenly distributed along the surface of the clay, leading to some intercalation and exfoliation. This means the N-TiO2-PILC has a larger SSA than nature clay and N-TiO2, which result in the higher adsorption capacity of Cr(VI) ions.

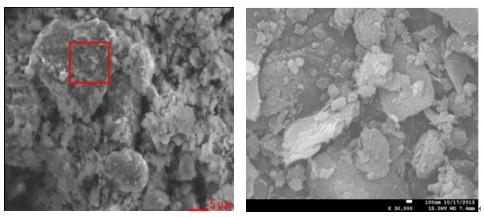

Figure 1: SEM images of purified nature clay (left) and N-TiO2-PILC (right)

3.2 XRD analysis

Figure 2 presents the XRD spectra of nature clay, N-TiO2-PILC calcined under 500 ºC (hereinafter referred to as N-TiO2-PILC-500 ºC), and N-TiO2-PILC calcined under 700 ºC (hereinafter referred to as N-TiO2-PILC-700 ºC). After pillaring, the diffraction peaks of the minerals within the nature clay (e.g. CaCO3 and Al) became

weaker while the diffraction peak of anatase TiO2 (101) appeared, indicating that TiO2 particles were successfully synthesized and inserted into the interlayer of the clay. However, when the calcination temperature increased to 700 ºC, SiO2 underwent a crystal transformation from quartz to moganite, and the diffraction peaks of the mineral within the nature clay became weaker than that of TiO2, revealing the destruction of interlayer structure. According to Scherrer equation, the grain sizes of N-TiO2-PILC-500 ºC and N-TiO2-PILC-700 ºC were 9.5nm and 17.4nm, respectively. Considering the negative correlation between grain size and photocatalytic activity, 500 ºC was proved to be the better calcination temperature.

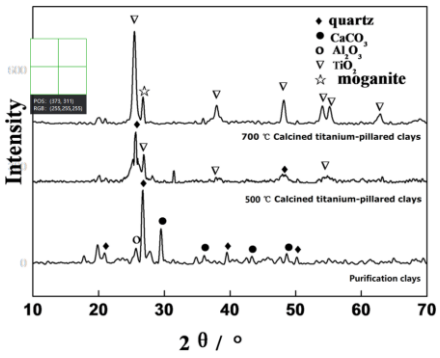

Figure 2: XRD spectra of Purified clay, N-TiO2-PILC-500 ºC and N-TiO2-PILC-700 ºC

3.3 EDS analysis

The elements of nature clay and N-TiO2-PILC are displayed in Figure 3 and Table 1. Many exchangeable cation ions (e.g. Fe, Mg, Al and Ca) were observable in the nature clay. After pillaring, the peaks of these ions became weaker, while the peak of Ti ions appeared. This means TiO2 particles have successfully replaced these ions and entered the interlayer of the clay.

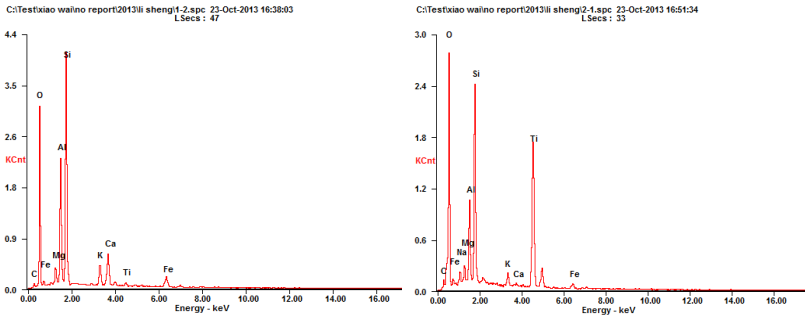

Figure 3: EDS spectra of Purified Clay (left) and N-TiO2-PILC (right)

Table1: Elemental analysis of Purified Clay and N-TiO2-PILC (Wt%: weight percentage; At%: atomic percentage)

Formula	Purification clay		Titanium-pillared clay	
	Wt%	*At%*	*Wt%*	*At%*
C	3.60	6.52	2.11	4.13
O	40.26	54.68	40.61	59.55
Na	——	——	1.39	1.42
Mg	2.17	1.94	0.95	0.91
Al	11.36	9.15	5.74	5.00
Si	24.25	18.76	14.14	11.81
K	2.74	1.52	1.42	0.85
Ca	8.54	4.63	0.34	0.20
Ti	0.87	0.40	30.67	15.02
Fe	6.20	2.41	2.62	1.10
Matrix	Correction	ZAF	Correction	ZAF

3.4 BET analysis

Figure 4 shows the N2 adsorption isotherms (left) and pore size distributions (right) of nature clay and N-TiO2-PILC. It can be seen that both curves follow the IV adsorption isotherm specified in IUPAC classification, revealing that the two samples share the same layered structure. Furthermore, N-TiO2-PILC had a more uniform distribution of pore size (10nm) than the nature clay.

Table 2 lists the BET analysis results of TiO2, N-TiO2, nature clay and N-TiO2-PILC. The results show that N-TiO2-PILC surpassed the other three samples in SSA, pore size and N2 adsorption capacity. Thus, this catalyst is expected to have a better adsorption ability for Cr(VI) ions than the others. The excellent ability is attributable to the entry of TiO2 particles into the interlayers of the clay, which caused intercalation and exfoliation, and in turn modified the surface structure of the sample.

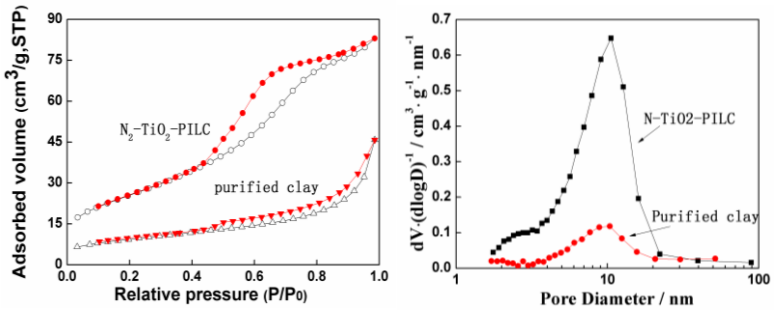

Figure 4: N2 adsorption isotherm (left) and pore size distribution (right) of purified clay and N-TiO2-PILC

Table2: BET data of different samples

Samples	S_{BET} ($m^2 \cdot g^{-1}$)	R_P (nm)	V_m ($cm^3 \cdot g^{-1}$ STP)	V_p ($cm^3 \cdot g^{-1}$)
TiO_2	3.41	9.60	0.78	0.008
N-TiO_2	15.35	8.09	3.53	0.031
Purified clay	32.95	8.60	7.57	0.071
N-TiO_2-PILC	93.16	5.52	21.40	0.128

4. Sample Performance Test

4.1 Dark adsorption

Figure 5 presents the time history of dark adsorption for Cr(VI) by nature clay, calcined nature clay, N-TiO2 and N-TiO2-PILC. It is evident that the N-TiO2-PILC-500°C boasted the best adsorption capacity for Cr(VI) after 40min, thanks to the huge SSA of N-TiO2-PILC as proved in the BET analysis. Furthermore, the inserted Ti ions pushed up the positive surface charge of the nature clay, creating an electrostatic attraction toward the Cr(VI) ions (which exist in the form of Cr2O72-) in water. When the reaction lasted for about 30min, all samples reached the adsorption equilibrium. Thus, photocatalytic reaction was carried out after 30min in darkness, aiming to eliminate the impact of adsorption.

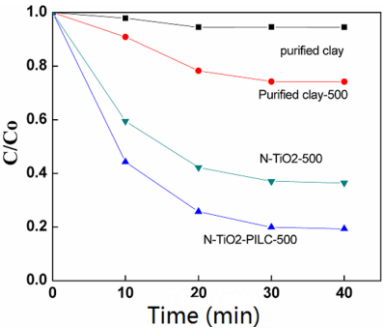

Figure 5: Dark adsorption for Cr(VI) by different samples

4.2 Effect of N-TiO2-PILC preparation conditions on Cr(VI) removal

Table 3 shows the effect of N-TiO2-PILC preparation conditions on Cr(VI) removal from water under visible light. At the beginning, the removal efficiency increased with the acid-base ratio and peaked at the ratio of 3:1. However, further growth in the acid-base ratio caused a decline in the removal efficiency. A possible reason lies in that, Ti particles were positively charged when the added base was deficient, making it difficult to produce the poly-condensation product ([(TiO)x(OH)y(H2O)z]n+). Subsequently, fewer Ti ions could be exchanged into the interlayer of the clay. The addition of the base weakened the electrostatic repulsion,

producing more [(TiO)x(OH)y(H2O)z]n+. These Ti groups replaced the cation ions in the clay and expanded the inter-lamellar space. However, an excessive amount of base would destroy the interlayer structure of the clay. Therefore, the optimal acid-base ratio was determined as 3:1.

Table 3 also presents the Cr(VI) removal efficiencies by N-TiO2-PILC prepared at different Ti/clay ratios. With the growth in the Ti/clay ratio, more and more Ti ions replaced the cation ions in the clay and entered the interlayer. The resulting increase in inter-lamellar space and the SSA enhanced the removal efficiency of Cr(VI) (Shi, R et al.,2017). Nonetheless, when the inserted Ti ions reached the saturation point, the redundant Ti ions started to inhibit the ion exchange and suppress the grain dispersion, lowering the removal efficiency from 90.2% to 76.9%. Therefore, the optimal Ti/clay ratio was proved to be 15mmol/g.

The Cr(VI) removal efficiency by N-TiO2-PILC calcined under different temperatures are listed on the right side of Table 3. It can be seen that the removal efficiency decreased with the rise in calcination temperature, especially after 500 ºC. There are two possible reasons for this trend. Firstly, as the temperature rose from 400 ºC to 500 ºC, more dehydroxylation reaction occurred and TiO2 grain size became smaller, leading to a relatively small inter-lamellar space. Thus, the adsorption ability of the nanocomposites exhibited a slight decrease. Secondly, further increase of the temperature would break the layer crystal structure of the clay, causing a sharp decline in adsorption ability and the photocatalytic activity.

To determine the optimal calcination temperature for N-TiO2-PILC, the amount of reduced Cr(III) ions in water was tested after 2h reaction according to the difference between the amount of redundant Cr(VI) and the amount of redundant total Cr. The amount of Cr(III) amount was 18μg, 116μg, 280μg and 614μg, respectively, for N-TiO2-PILC calcined under 400 ºC, 500 ºC, 600 ºC and 700 ºC. This is because the TiO2 gradually transformed from amorphous phase into anatase phase under the rising calcination temperature (Chen et al., 2017). Since the anatase phase is more favourable for photo-activity, the photocatalytic reduction was promoted by the elevated calcination temperature. Considering the adsorption ability and the photo-activity, 500 ºC was selected as the optimal calcination temperature.

Table3: Cr(VI) removal efficiency by N-TiO2-PILC prepared under different conditions

acid-base ratio	Efficiency (%)	Ti/clay ratio (Mmol/g)	Efficiency (%)	Calcination temperature	Efficiency (%)
4:1	87.1	12.5	76.7	400 ºC	93.7
3:1	90.2	15	90.2	500 ºC	90.2
2:1	76.9	18	82.2	600 ºC	75.1
1.6:1	40.2	25	76.9	700 ºC	38.0

4.3 Effect of pillaring on Cr(VI) removal

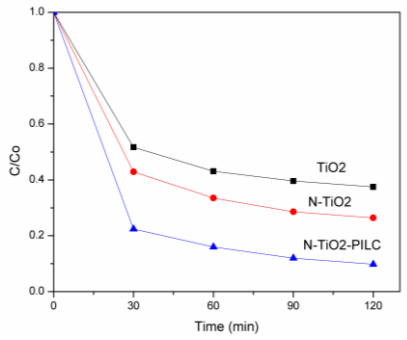

Figure 6: Time history of Cr(VI) removal by TiO2, N-TiO2 and N-TiO2-PILC

Figure 6 shows the time history of Cr(VI) removal by TiO2, N-TiO2 and N-TiO2-PILC. The catalysts were ranked as TiO2 < N-TiO2 < N-TiO2-PILC in descending order of removal efficiency. The N-TiO2 outshined the original TiO2 in photo-activity, probably because of its stronger visible light absorption and larger SSA caused by N-insertion. After 2h reaction, N-TiO2-PILC composite achieved the highest removal efficiency (90.2%), thanks to its large surface and low hole-electron recombination ratio resulted from the electron transition between N-TiO2 and clay. Thus, it is concluded that N-TiO2-PILC has an edge over the other two catalysts in terms of photo-activity.

4.4 Effect of pillaring on the settleability

The turbidity of the reaction mixture containing different catalysts was tested after standing for 24h, and the results were recorded in Table 4 below. As shown in the table, the solutions containing TiO2 and N-TiO2 remained turbid after 24h, while the solution containing N-TiO2-PILC as clear as distilled water. The good settleability of the latter solution must be enhanced by the composition of nature clay and N-TiO2, probably due to the strong coagulation ability of the clay.

Table 4: Turbidity of solutions containing different catalysts after 24h

Sample	TiO_2	N-TiO_2	N-TiO_2-PILC
Turbidity (NTU)	2890.0	2480.0	12.4

4.5 Effect of pillaring on reusability

The stability and reusability of photocatalysts directly bear on their practical application in Cr(VI) removal. Hence, the author tested the reusability of TiO2, N-TiO2 and N-TiO2-PILC under the same conditions. After each cycle, the catalysts were collected by centrifugation, washed by deionized water and then dried under 80 ºC overnight. The regenerated materials were applied in Cr(VI) solutions in the dosage of 5g/L. Through the tests, TiO2 and N-TiO2 lost all of their effects after two cycles, while Cr(VI) removal efficiency of N-TiO2-PILC remained above 65.5% after 5 cycles, indicating that pillaring can greatly enhance the reusability of TiO2.

5. Conclusions

Through XRD and EDS analysis of modified N-TiO2-PILC samples, it is concluded that, after pillaring, the TiO2 particles successfully replaced the cation ions in the clay and entered the interlayer. These particles were well dispersed as per the results of SEM analysis. In addition, BET analysis shows the increased pore volume and SSA of the composites after pillaring, while the pore size became smaller and more uniform.

During photo-reduction experiments, the optimal preparation conditions of N-TiO2-PILC was confirmed according to the removal efficiency of Cr(VI). The optimal acid-base ratio and Ti/ clay ratio were determined as 3:1mL/mL and 15:1mmol/g, respectively; the optimal calcination temperature was proved to be 500 ºC. Compared to unmodified samples, N-TiO2-PILC enjoys good adsorption ability and photo-activity for Cr(VI) removal under visible light. Furthermore, the settleability and reusability of the samples were also improved through pillaring.

Acknowledgments

This work was financially supported by Fundamental Research Funds for the Central Universities (Grant No: 2017 MS136).

References

Chen J., Wang X., Li Y., Zhang N., Su M., Han J., 2017, Photocatalytic activity of synthetic n-doped tio2/reducedgraphene oxide crystalline composites, Chemical Engineering & Technology, 40(7), 1347-1353, DOI: 10.1002/ceat.201600671

Han C., Tian J., Zhang J., He Y., 2018, Effects of different porosities on shear strength of fiber clay by response surface methodology, Chemical Engineering Transactions, 66, 1111-1116. DOI:10.3303/CET1866186

Hu J., Li H., Muhammad S., Wu Q., Zhao Y., Jiao Q., 2017, Surfactant-assisted hydrothermal synthesis oftio2/reduced graphene oxide nanocomposites and their photocatalytic performances, Journal of Solid State ChemistryFrance, 253, 113-120, DOI: 10.1016/j.jssc.2017.05.034

Shi R., Li Z., Yu H., Shang L., Zhou C., Gin W., 2017, Effect of nitrogen doping level on the performance ofn-doped carbon quantum dot/tio2 composites for photocatalytic hydrogen evolution, Chemsuschem, 10(22), 4650-4656, DOI: 10.1002/cssc.201700943

Wang G., Ma X., Wang C., Li S., Qiao J., Zhang H., 2018, Highly efficient visible-light driven photocatalytichydrogen evolution over Er 3+ :yalo 3 /Ta 2 O 5 /rgo/mose 2, nanocomposite, Journal of Molecular Liquids, 260, 375-385, DOI: 10.1016/j.molliq.2018.03.110

Xu H., Zhang L., 2017, Selective nonaqueous synthesis of c-cl-codoped tio2 with visible-light photocatalyticactivity, Guangdong Chemical Industry, 114(26), 11534-11541, DOI: 10.1021/jp1027965

Zhou L., Wang L., Lei J., Liu Y., Zhang J., 2017, Fabrication of tio2/co-g-c3n4 heterojunction catalyst and itsphotocatalytic performance, Catalysis Communications, 89, 125-128, DOI: 10.1016/j.catcom.2016.09.022